Floquet analysis of quantum resonance in a driven nonlinear system

Ju-Yong Shin and Hai-Woong Lee

Department of Physics, Korea Advanced Institute of Science and Technology, Taejon 305-701, Korea

(Received 7 March 1994)

The characteristics of quantum resonance induced in a nonlinear system driven by a periodic force are studied based on the Floquet formalism through theoretical analysis and numerical computation of quasienergies and quasienergy states. Particular attention is given to those characteristics that separate quantum resonance from the corresponding classical resonance, and their implication to the problem of resonance overlap is considered. As an illustration, numerical data are presented for a particle in an infinite square well potential driven by a sinusoidal force.

PACS number(s): 05.45.+b, 47.52.+j, 03.65.Sq

I. INTRODUCTION

The concept of resonance plays an important role in one's understanding of the classical chaotic dynamics of a driven nonlinear system. In particular, it is well known that the overlap between resonance zones induced in the system by the driving force can serve as a criterion for the onset of classical chaos [1, 2]. Recent investigations [3–5] have indicated that the quantum dynamics of a nonlinear system can also be described in a coherent fashion in terms of resonance. Study of quantum resonance and the role it plays in a quantized nonlinear system should therefore shed light on the difficult issue of the quantum-classical correspondence or noncorrespondence in the dynamics of nonintegrable systems.

Resonance arises from a local coupling of energy states. The behavior of all levels coupled to form a resonance zone collectively determines the characteristics of that resonance, which in turn determines the quantum dynamical behavior of the system. When considering a system driven by a periodic force, study of the structure of the quasienergies and quasienergy states [6–9] bears importance because all information on the characteristics of quantum resonance is contained in them.

The primary purpose of this work is to investigate the quantum dynamics of a nonlinear system driven by a periodic force based on the Floquet formalism [6–11]. Particular emphasis is given to the resonances, their formation process and characteristics, induced in the system by the driving force, as manifested in the quasienergies and in the probability distribution of quasienergy states. We are particularly interested in the characteristics of quantum resonance that differ from those of the corresponding classical resonance, because they form the basis for our study of the quantum-classical correspondence in relation to the well-known phenomenon of the quantum suppression of classical chaos [12–16].

For our description of quasienergy states, we adopt the phase-space representation which has found much use recently in studies of classically chaotic systems [10,11,17–27]. Contour plots of the quantum phase-space distribution function are the natural quantum analog to the classical Poincaré map and thus are capable of clearly exhibiting the structure of quantum resonance zones that are formed in the system. We, in particular, choose to use contour plots of the Husimi distribution function [28, 29] which is obtained by smoothing the Wigner distribution function [30] with a Gaussian wave packet. Due to Gaussian smoothing, the Husimi plots are generally simpler in structure than the Wigner plots and yet contain all physically meaningful information that the Wigner plots have, and thus are best suited to study classically chaotic systems having complex phase-space structures.

Our analysis is based largely upon numerical data which are obtained from computations performed on a specific system; namely, a particle in an infinite square well potential driven by a sinusoidal force. Investigations on both the classical and quantum dynamics of this system were already reported in the past [5,31–33]. The system has perhaps the simplest resonance structure among driven nonlinear systems, and an analytic formula exists [5] that gives an approximate estimate of the quasienergies of this system which can be used to help interpret our numerical data. Our numerical computation of the quasienergies and quasienergy states is performed as follows. We first obtain the matrix element U_{nm} of the time evolution operator U by numerically integrating the Schrödinger equation from time $t = 0$ to $t = T$ (T is the period of the external force) subject to the initial condition $\psi(t = 0) = u_m$ and computing the transition amplitude $\langle u_n|\psi(t = T)\rangle$, where u_n refers to the nth eigenstate of the unperturbed Hamiltonian. Once all U_{nm}'s are obtained, the quasienergies ϵ_n and corresponding quasienergy states χ_n are given essentially as eigenvalues and eigenstates of U according to the equation

$$U\chi_n = e^{-i\epsilon_n T/\hbar}\chi_n. \tag{1}$$

The system parameters we choose for our computation are $\hbar = 1$, m (mass of the particle) $= 1$, $2a$ (width of the potential well) $= 6$, and ω (frequency of the external force) $= 5$. For the computation of Husimi plots, we choose to smooth the Wigner distribution function with a minimum uncertainty wave packet with the coarse-graining parameter [11, 23, 29] of 1.56. This parameter

determines the relative resolution of the Husimi plot in q vs p space.

In Secs. II and III, we carry out analysis and computation of the quasienergy states and quasienergies, respectively. Information on the characteristics of the quantum resonance obtained based on the analysis and computation is then used in Sec. IV to discuss the resonance overlap in quantum systems in relation to the phenomenon of the quantum suppression of classical chaos.

II. QUASIENERGY STATES AND THE FORMATION OF QUANTUM RESONANCE

Let us consider a nonlinear system driven by a sinusoidal force so that the total Hamiltonian for the system is $H = H_0 + qF_0 \cos \omega t$. We wish to study changes that occur in the quasienergy states as the amplitude F_0 of the force is increased. Let u_n and χ_n denote, respectively, the nth eigenstate of the unperturbed Hamiltonian H_0 and the corresponding quasienergy state. At an extremely low value of F_0, one may neglect the coupling between all states except for the two, say u_N and u_{N+1}, that most closely meet the resonance condition. The two quasienergy states that result from the coupling of u_N and u_{N+1} can be written as

$$\chi_N = u_N \cos\theta + u_{N+1} \sin\theta, \tag{2}$$

$$\chi_{N+1} = u_{N+1} \cos\theta - u_N \sin\theta, \tag{3}$$

where θ is the parameter that measures the strength of the coupling. As a result of the coupling, the two states u_N and u_{N+1} are redistributed slightly in phase space. If all other levels are far from resonance, we have, in the limit $F_0 \to \infty$,

$$\chi_N = \frac{1}{\sqrt{2}}(u_{N+1} + u_N), \tag{4}$$

$$\chi_{N+1} = \frac{1}{\sqrt{2}}(u_{N+1} - u_N). \tag{5}$$

Thus, the quasienergy states χ_N and χ_{N+1} are symmetric and antisymmetric combinations of u_N and u_{N+1}.

In realistic situations, usually more than two levels are coupled and quasienergy states are given by combinations of all coupled states. Some general treatment of these quasienergy states is still possible with the help of appropriate approximations. For example, the dynamics in a given resonance zone can be approximated by that subject to a pendulum potential, if effects of other resonances are neglected, i.e., if the single resonance approximation is made. The quasienergy states of the system should then resemble eigenstates of the Mathieu equation [5]. Detailed discussion is of course more complex than that for the two-level case. Despite the complexity, however, the probability distribution of the quasienergy states should contain information on the coupling between different energy levels and thus on the structure of the resonance induced by the coupling.

As an example, let us consider a particle of mass m in a symmetric infinite square well potential of width $2a$ driven by a sinusoidal force $F = F_0 \cos \omega t$. The data presented in this work are obtained with the parameter $\hbar = 1$, $m = 1$, $a = 3$, and $\omega = 5$, while several different values of F_0 are used. The classical phase-space map of the system is shown in Figs. 1(a) and 1(b) for the cases $F_0 = 2$ and $F_0 = 6$, respectively. The period-1 primary resonance centered at the elliptic fixed point, $q = -a, p \simeq \pm 2am\omega/\pi$, is clearly visible. The hyperbolic fixed point is located on the other side of the well, i.e., at $q = a$, $p \simeq \pm 2am\omega/\pi$. Quantum mechanically, the nth eigenstate u_n of the unperturbed Hamiltonian H_0 is given by

$$u_n = \frac{1}{\sqrt{a}} \sin\left[\frac{n\pi}{2a}(q + a)\right] \tag{6}$$

with energy $E_n = n^2\pi^2\hbar^2/(8ma^2)$. The two levels which come closest to resonance are u_{18} and u_{19}, when the parameter values listed above are chosen. In Fig. 2 we show contour plots of the Husimi distribution function for the four quasienergy states χ_{17} through χ_{20} for the case of a weak force, $F_0 = 0.04$. The quasienergy states are computed numerically according to the method described in the previous section. It can be seen that the quasienergy states χ_{17} and χ_{20} are essentially the same as the unperturbed eigenstates u_{17} and u_{20}, but χ_{18} has a probability distribution shifted slightly toward the elliptic fixed point compared with the probability distribution of u_{18}, and χ_{19} has it shifted slightly toward the hyperbolic fixed point compared with the probability distribution of u_{19}. This is consistent with Eqs. (2) and (3): with u_n defined as in Eq. (6) (to the immediate right of the left wall, $q = -a$, u_n is positive for all n), when u_N and u_{N+1} are added to (subtracted from) each other, one obtains a higher probability density in the region near the left

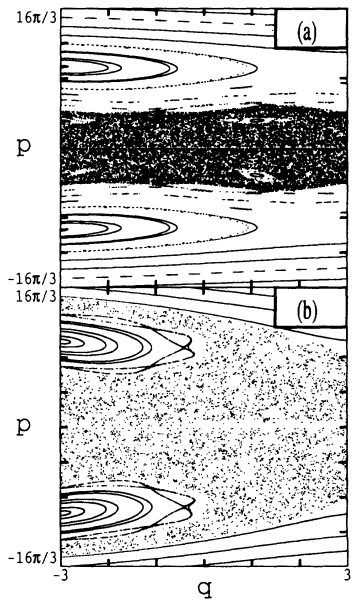

FIG. 1. Classical phase-space map of a particle of mass m in a symmetric infinite square well potential of width $2a$ driven by a sinusoidal force $F = F_0 \cos \omega t$. The parameters are chosen to be $m = 1$, $2a = 6, \omega = 5$. The amplitude of the driving force is $F_0 = 2$ for (a) and $F_0 = 6$ for (b).

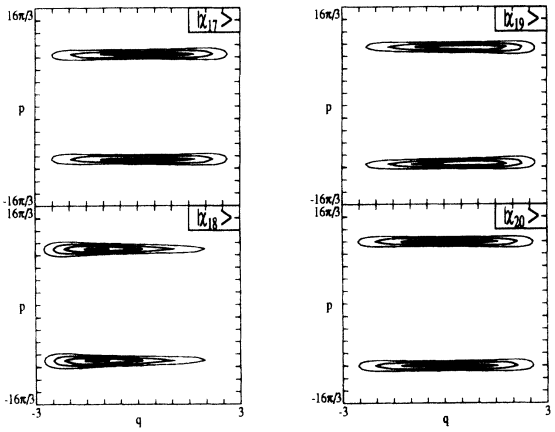

FIG. 2. Husimi plots of the quasienergy states χ_{17} through χ_{20} for the same system as in Fig. 1. The amplitude of the driving force is $F_0 = 0.04$, and $\hbar = 1$.

Further insight into the characteristics of localized and extended quasienergy states is provided by Fig. 4 in which the coefficients $b_{nm} = \langle \chi_n | u_m \rangle$ vs m are plotted for each χ_n ($n = 14$–23) for our square well system for the case $F_0 = 2$. We recall that, depending on whether b_{nm} and $b_{n,m+1}$ have the same sign or opposite signs, the probability density is enhanced near the left or right wall of the well when u_m and u_{m+1} are superposed. For the localized state χ_{18}, we see that all the coefficients $b_{18,m}$ are positive. Thus all pairs of the eigenstates u_m and u_{m+1} are superposed in such a way that the probability density is enhanced near the left wall and reduced near the right wall, resulting in a strongly localized distribution centered at the elliptic fixed point. For extended states, on the other hand, different pairs of eigenstates are superposed in such a way that the probability density is enhanced in different regions of phase space corresponding to the separatrix. For example, for χ_{15} the coefficients $b_{15,m}$ and $b_{15,m+1}$ have the same sign for $m = 13, 23$,

(right) wall and a lower probabilty density near the right (left) wall. This slight redistribution of the probability density can be regarded as a first step toward the formation of resonance. At this point, however, there is no evidence in the plot that suggests that resonance is formed. A clear indication of the formation of resonance can be found in Fig. 3, where the Husimi plots for χ_{14} through χ_{23} are presented at a higher value of the force amplitude, $F_0 = 2$. Again, the quasienergy states plotted are computed numerically according to the method described in the previous section. All quasienergy states χ_n plotted have their probability densities redistributed with respect to the corresponding unperturbed eigenstates u_n, which means that all the states u_{14} through u_{23} are coupled by the external force. Some quasienergy states such as χ_{18} and χ_{19} are peaked near the elliptic fixed point and have strongly localized distributions. Some other quasienergy states such as χ_{14}, χ_{15}, χ_{22}, and χ_{23} are peaked at a point closer to the hyperbolic fixed point and have more delocalized distributions. Clearly, the state χ_{18} is the ground state of the Mathieu equation while states with more delocalized distributions, which we call "extended" states, correspond to higher-lying excited states [34]. In other words, localized quasienergy states have the characteristics of the classical periodic orbits near the elliptic fixed point, while extended quasienergy states correspond to the classical behavior near the separatrix. The degree of the quantum-classical correspondence is thus seen to be strong at $F_0 = 2$. It is clear that, in order for quantum resonance to be formed and for the quantum-classical correspondence to be strong, the external force needs to be sufficiently strong to couple more than a few energy levels. Only when the redistribution of the probability density occurs among a sufficiently large number of levels can the quasienergy states have the localized or extended distributions and show the characteristics of resonance similar to those of the classical resonance. We emphasize that the coexistence of the localized and extended quasienergy states is a strong indication for the formation of quantum resonance.

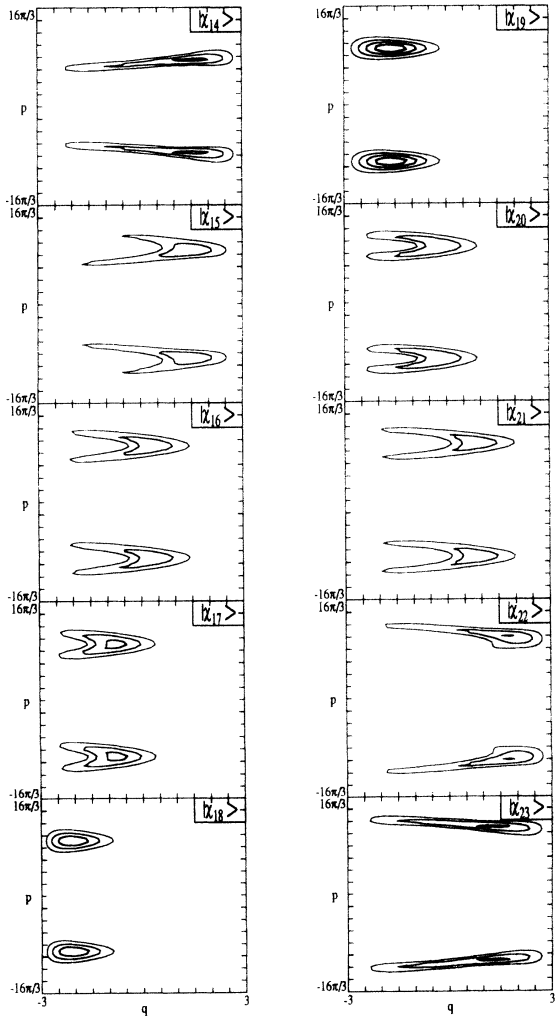

FIG. 3. Husimi plots of the quasienergy states χ_{14} through χ_{23} for the same system as in Fig. 1. The amplitude of the driving force is $F_0 = 2$, and $\hbar = 1$.

and 24 but opposite signs for $m = 16, 17$, and 18, leading to an enhancement of the probability density along the separatrix of the resonance.

Another set of data that shows distinction between the localized and extended quasienergy states is provided in Fig. 5, where the Husimi plots of the localized state χ_{18} and the extended state χ_{14} are shown at four different values of F_0; F_0 =1, 2, 3, and 4. There is very little change in χ_{18} as F_0 is increased from $F_0 = 1$ to $F_0 = 4$, whereas the extended state χ_{14} is seen to vary rather sensitively with respect to F_0. This is because χ_{14} lies largely outside the resonance zone and beyond the influence of the driving force at $F_0 = 1$, but occupies the separatrix region of the resonance at a higher value of F_0.

In summary of this section, we have seen that the formation of quantum resonance is accomplished when the external force is strong enough to couple a sufficiently large number of energy levels into localized and extended quasienergy states. Localized and extended quasienergy states are the quantum analog of periodic orbits near the elliptic fixed point and the separatrix, respectively, of the classical phase-space map.

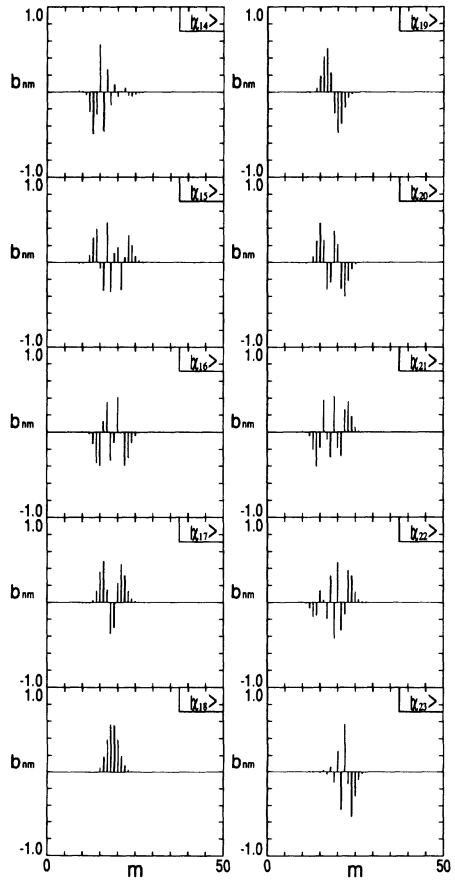

FIG. 4. The coefficients $b_{nm} = \langle \chi_n | u_m \rangle$ for the quasienergy states χ_n of Fig. 3.

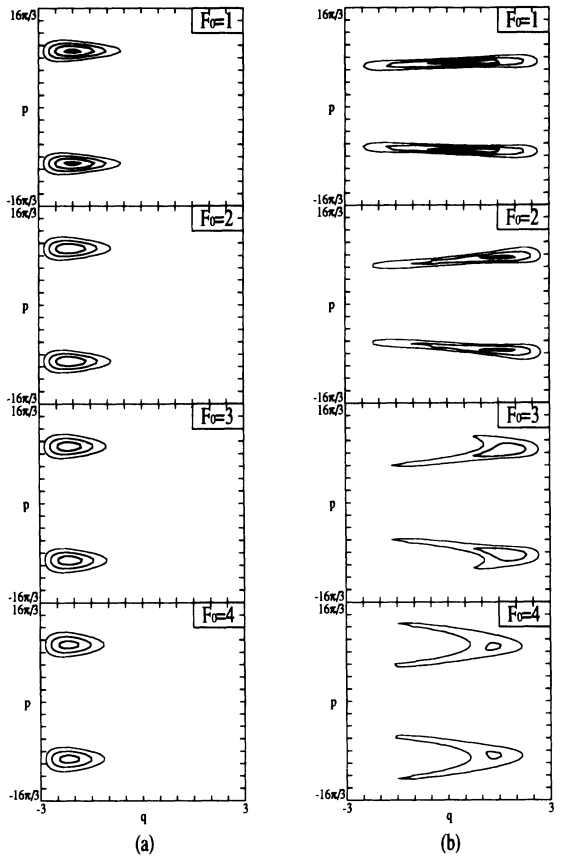

FIG. 5. Husimi plots of χ_{18} and χ_{14} shown in (a) and (b), respectively, at four different force amplitudes, F_0 = 1, 2, 3, and 4, for the same system as in Fig. 1. $\hbar = 1$.

III. QUASIENERGIES AND THE CHARACTERISTICS OF QUANTUM RESONANCE

In this section we show how one can obtain information about the characteristics of quantum resonance through investigation of quasienergies. Before considering the quasienergy, it is worthwhile to look at the quantity $\langle \chi_n | H_0 | \chi_n \rangle$, the expectation value of the unperturbed Hamiltonian. Equations (2) and (3) indicate that the coupling by the external force pulls the expectation value of the two states χ_N and χ_{N+1} somewhat closer to each other. Furthermore, Eqs. (4) and (5) suggest that, in the strong-coupling limit, quasienergy states in the same resonance zone have nearly the same expectation value $\langle \chi_n | H_0 | \chi_n \rangle$. Hence, the plot of $\langle \chi_n | H_0 | \chi_n \rangle$ vs n should give a rough estimate of the number of levels coupled in a resonance zone. As an illustration, we present in Fig. 6 the plot of $\langle p_n \rangle = \sqrt{2m \langle \chi_n | H_0 | \chi_n \rangle}$ for our system of the driven particle in an infinite square well potential for different values of the force amplitude F_0. Resonance zones are represented by the flat regions in each curve. The flat region centered at $n \simeq 18$ in each curve is the period-1 primary resonance. One can clearly see that the width of the resonance increases with F_0. There also is

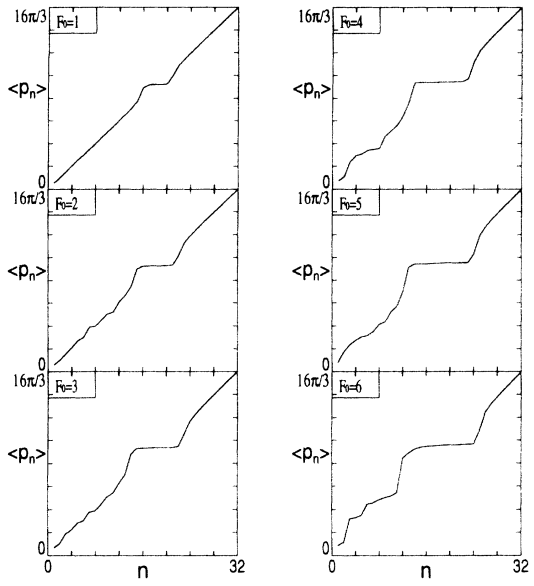

FIG. 6. $\langle p_n \rangle = \sqrt{2m\langle \chi_n | H_0 | \chi_n \rangle}$ vs n at six different force amplitudes, $F_0 = 1$, 2, 3, 4, 5, and 6, for the same system as in Fig. 1. $\hbar = 1$.

an indication of the presence of the period-3 primary resonance zone in the neighborhood of $n \simeq 6$ at high values of F_0 ($F_0 \geq 4$). In principle, even higher-period primary resonances can be formed centered at lower values of n, but the formation of these resonances is restricted by the discrete nature of the energy levels, i.e., by the fact that there are only a limited number of levels available to form these resonances. High-order resonances are also difficult to form. As described in the previous section, resonance is formed when the external force is large enough to couple a sufficiently large number of levels. The higher the order of the resonance is, the greater is the magnitude of the external force needed to couple a given number of levels. Furthermore, high-order resonances often exist in the neighborhood of lower-order resonances, and energy levels that are coupled to form a lower-order resonance are not available to a higher-order resonance. Thus the number of levels that can contribute to form high-order resonances is limited. One can therefore conclude that the degree of the quantum-classical correspondence is generally weaker for higher-period higher-order resonances, i.e., the role played by higher-period higher-order resonances is weaker in a quantum system than in the corresponding classcial system.

Let us turn our attention now to the quasienergy. One quantity that can conveniently describe the structure of the quasienergy is the "quasifrequency" defined as

$$\Delta\omega_n = \frac{\epsilon_n - \epsilon_{n-1}}{\hbar}, \tag{7}$$

where ϵ_n is the quasienergy associated with the nth quasienergy state χ_n. In order to help understand the physical significance of the quasienergy and quasifrequency, we calculate the quasienergies and quasifrequencies for our system of a driven particle in an infinite square well potential. An estimate of quasienergies can be obtained using the approximate formula given by Lin and Reichl [5],

$$\epsilon_n = \frac{1}{4}\alpha_{j(n)}\hbar\Omega_0 - \frac{\hbar\omega^2}{4\Omega_0} + n\hbar\omega, \tag{8}$$

where $\Omega_0 = \pi^2\hbar/(8ma^2)$, $\alpha_{j(n)}$ is the jth eigenstate of the Mathieu equation

$$\frac{1}{2}\frac{d^2U_\alpha(\theta)}{d\theta^2} + \frac{\alpha}{2}U_\alpha(\theta) + \rho\cos(2\theta)U_\alpha(\theta) = 0, \tag{9}$$

and $\rho = 8aF_0/(\pi^2\hbar\Omega_0)$. The subscript $j(n)$ in $\alpha_{j(n)}$ indicates that once n is given j is determined. For the system being considered, for which χ_{18} is the ground state of the Mathieu equation, n runs in the order $18, 19, 17, 20, \ldots$, corresponding to $j = 0, 1, 2, 3, \ldots$. The quasifrequency $\Delta\omega_n$ is obtained immediately from Eqs. (7) and (8) as

$$\Delta\omega_n = \omega + \frac{\Omega_0}{4}\left[\alpha_{j(n)} - \alpha_{j'(n-1)}\right]. \tag{10}$$

Equations (8) and (10) are valid under the single resonance approximation, i.e., these equations are valid when effects of other resonances are neglected. While Eqs. (8) and (10) yield an approximate evaluation of the quasienergies and quasifrequencies for our system, an accurate computation of quasienergies and quasifrequencies can be performed using the numerical method described in Sec. I. Results of such a computation are presented in Fig. 7 in which the quasifrequencies computed at $F_0 = 2$ are represented by circles. In the absence of the external force, the quasifrequency for the present system increases linearly with respect to n as indicated by the dashed line in Fig. 7. The difference between the circles and the dashed line may be considered to represent effects of the external force.

The physical significance of Fig. 7 can best be seen by considering the system in the classical limit. In the classical limit, the Mathieu equation is replaced by the pendulum equation

$$\frac{1}{2}\left(\frac{d\theta}{dt}\right)^2 - \rho\cos 2\theta = \frac{\alpha}{2}, \tag{11}$$

and Eq. (10) takes the form

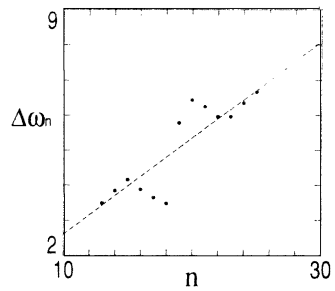

FIG. 7. The quasifrequency $\Delta\omega_n$ vs n at the force amplitude $F_0 = 2$ for the same system as in Fig. 1. The circles are the quasifrequencies computed numerically and the dashed line represents the quasifrequency in the limit $F_0 = 0$. $\hbar = 1$.

$$\Delta\omega(I) = \omega + \frac{I - I_0}{|I - I_0|}\frac{\Omega_0}{4}\Omega(2|I - I_0|), \tag{12}$$

where I denotes the classical action variable, I_0 is the action corresponding to the period-1 primary resonance given by $I_0 = n_0\hbar$, $n_0 = 4ma^2\omega/(\pi^2\hbar) \simeq 18.2$, and $\Omega(2|I - I_0|)$ is the frequency of the motion of the classical particle of action $(2|I - I_0|)$ moving in the pendulum potential. In Fig. 8 we show a plot of $\Delta\omega$ as a function of I calculated from Eq. (12) for the case $F_0 = 2$. We note that, at two values of I ($I = 12.2$ and 24.2) corresponding to the two values of momentum at the separatrix, the quasifrequency becomes equal to the frequency ($\omega = 5$) of the driving force. This can be understood by noting that the period of the classical motion at the separatrix is infinitely long and thus, taking $\Omega \to 0$ in Eq. (12), $\Delta\omega$ becomes equal to ω. Clearly, the width of the resonance zone in the classical limit, which can be defined as the size of the action region bounded by the separatrix, is given by 24.2−12.2=12 at $F_0 = 2$.

Let us now go back to Fig. 7. We first note the similarity in shape of the $\Delta\omega_n$ vs n curve in Fig. 7 and the $\Delta\omega$ vs I curve in Fig. 8, which can be regarded as a strong indication for the existence of the period-1 primary resonance zone in the quantum system. We note, however, that the quantum quasifrequency $\Delta\omega_n$ does not become quite equal to the frequency of the driving force even for the extended quasienergy states. One can see this also from the approximate formula, Eq. (10), according to which

$$\Delta\omega_n - \omega = \frac{\Omega_0}{4}\left[\alpha_{j(n)} - \alpha_{j'(n-1)}\right]. \tag{13}$$

This equation indicates that the discrete nature of the quasienergy levels keeps the quasifrequency $\Delta\omega_n$ from becoming equal to the frequency of the external force. It nevertheless is still possible to estimate the size of the quantum resonance zone from Fig. 7, because the resonance zone can reasonably be considered to be bounded by two extended quasienergy states for which the quasifrequency takes on a value closest to the frequency of the driving force. From Fig. 7 and also from Fig. 3 we see immediately that the two extended quasienergy states are χ_{15} and χ_{23} (or possibly χ_{22}), yielding the width of the quantum resonance zone to be $23-15 \simeq 8$. This width of the quantum resonance zone is smaller than the width (~ 12) of the corresponding classical resonance zone estimated above. The smaller width of the quantum resonance compared with that of the corresponding classical resonance has important bearings on the issue of "quantum chaos." The smaller the width of each resonance zone is, the less likely two neighboring resonance zones are to overlap. The quantum suppression of classical chaos is thus suggested.

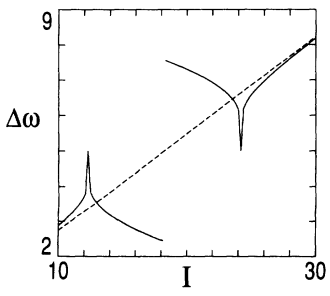

FIG. 8. The classical quasifrequency $\Delta\omega$ vs the action variable I at $F_0 = 2$ for the same system as in Fig. 1. The solid curves are the classical quasifrequencies and the dashed line represents the classical quasifrequency in the limit $F_0 = 0$.

In summary, we have shown that the $\Delta\omega_n$ vs n curve offers a convenient means of studying the characteristics of quantum resonance. It shows that quantum resonance has a similar structure to the corresponding classical resonance although the quantum quasifrequency does not become quite equal to the frequency of the driving force. It shows also that, at least for our model of the driven particle in a square well potential, the width of the quantum resonance is smaller than that of the corresponding classical resonance. We have also shown in this section that high-period, high-order resonances play a weaker role in quantum systems than in the corresponding classical systems.

IV. QUANTUM SUPPRESSION OF CLASSICAL CHAOS

It is well known that the overlap between two neighboring resonances for a classical system signals the onset of classical chaos [1, 2]. Since the overlap occurs between periodic orbits near the separatrixes of two resonances, classical chaos can be regarded as being initiated in the separatrix region of the resonances. We have seen in Sec. II that the quantum analog of periodic orbits near the separatrix is the quasienergy states having extended probability distributions. Thus the resonance overlap in a quantum system can be seen as a coupling between extended quasienergy states belonging to two neighboring quantum resonances.

So far in our study of quasienergy states and quasienergies, we have seen some indications that the overlap between quantum resonances would not occur as easily as that between classical resonances. According to the renormalization theory [2, 35], in a classical system the resonance overlap is initiated by high-period high-order resonances. In a quantum system, however, high-period high-order resonances cannot easily be formed, because only a limited number of levels are available to form the resonances and, even if there are a sufficient number of levels, a strong external force is required to couple them. Furthermore, our computation on the model of the square well system suggests that the width of the quantum resonance is smaller than that of the classical resonance of the same period and order at the same value of the force amplitude. Thus the condition for the overlap of two neighboring resonances seems to be more difficult to be met in a quantum system than in the corresponding classical system.

The question still remains, however, as to the behavior of a quantum system at a very high value of the force amplitude, say at $F_0 = 6$, at which a significant portion of the classical phase space is occupied by the chaotic

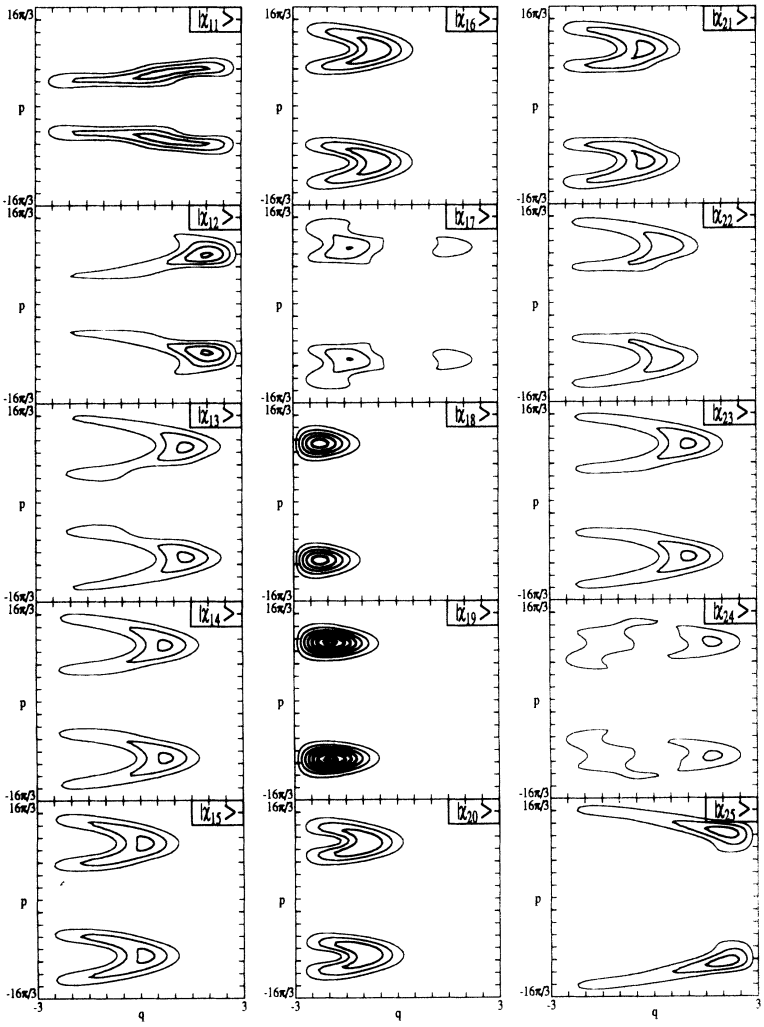

FIG. 9. Husimi plots of the quasienergy states χ_{11} through χ_{25} for the same system as in Fig. 1. The amplitude of the driving force is $F_0 = 6$, and $\hbar = 1$.

sea as shown in Fig. 1(b). A partial answer to this question can be found in Fig. 9 where the Husimi plots of the quasienergy states χ_{11} through χ_{25} at $F_0 = 6$ for the driven particle in an infinite square well potential are shown. One observes that all quasienergy states still have some distinct peaks at $F_0 = 6$ and thus that no quasienergy state is truly delocalized, i.e. there is no trace in this plot that suggests any chaotic behavior. This is, of course, consistent with earlier observations of the quantum suppression of classical chaos [12–16].

Further data to support the above observation are given in Figs. 10(a) and 10(b) in which the quantum Poincaré map of the Husimi distribution function

$$\overline{H(q,p)} = \frac{1}{N}\sum_{n=0}^{N-1} H(q,p,nT) \tag{14}$$

is shown at $F_0 = 6$ with $N = 110$ for our system of the driven particle in an infinite square well potential. Figures 10(a) and 10(b) were obtained with the initial states whose Husimi plots are given by Figs. 10(c) and 10(d), respectively. Fig. 10(c) represents a wave packet localized in the neighborhood of the elliptic fixed point of the

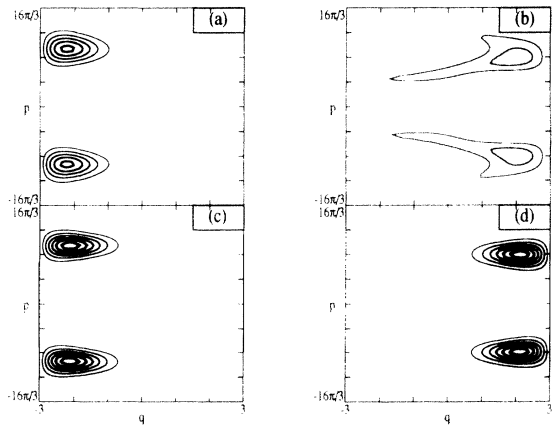

FIG. 10. Quantum Poincaré maps, (a) and (b), of the Husimi distribution function for the same system as in Fig. 1. The amplitude of the driving force is $F_0 = 6$, and $\hbar = 1$. The initial wave packet is assumed to be centered near the elliptic fixed point of the primary resonance for (a) and the hyperbolic fixed point of the primary resonance for (b). Husimi plots of the initial wave packet for (a) and (b) are shown in (c) and (d), respectively.

period-1 primary resonance zone, while Fig. 10(d) is a wave packet localized near the hyperbolic fixed point of the same resonance zone. One sees clearly from Fig. 10 that in the former case the probability tends to remain localized near the initial distribution, while in the latter there is some spreading of the probability distribution over states not initially populated. It should be noted that in the latter case the probability density near the elliptic fixed point of the resonance zone remains small, indicating clearly that the initial wave packet is affected by the presence of the resonance zone. More importantly, in either case we do not see any significant penetration of the probability density into the neighboring resonance zone, in particular into the period-3 primary resonance zone which is centered at $p \simeq \pm 3.2$ or $n \simeq 6.1$. Furthermore, the quantum Poincaré maps in both cases exhibit the two-peak structure, suggesting strongly that the nature of the quantum motion is regular rather than chaotic. A strong quantum-classical noncorrespondence is evident in case the initial wave packet is given by Fig. 10(d), because the center of this initial wave packet is located within the classically chaotic region. All our observations are thus consistent with the notion of the quantum suppression of classical chaos.

ACKNOWLEDGMENTS

This research is supported in part by the Korea Science and Engineering Foundation and by KAIST Research Grant.

[1] B. V. Chirikov, Phys. Rep. **52**, 263 (1979).
[2] D. F. Escande, Phys. Rep. **121**, 165 (1985).
[3] G. P. Berman and G. M. Zaslavsky, Phys. Lett. **61A**, 295 (1977).
[4] G. M. Zaslavsky, Phys. Rep. **80**, 157 (1981).
[5] W. A. Lin and L. E. Reichl, Phys. Rev. A **37**, 3972 (1988).
[6] Ya. B. Zel'dovich, Zh. Eksp. Teor. Fiz. **51**, 1492 (1966) [Sov. Phys. JETP **24**, 1006 (1967)].
[7] H. Sambe, Phys. Rev. A **7**, 2203 (1973).
[8] Ya. B. Zel'dovich, Usp. Fiz. Nauk. **110**, 139 (1974) [Sov. Phys. Usp. **16**, 427 (1974)].
[9] N. L. Manakov, V. D. Ovsiannikov, and L. P. Rapoport, Phys. Rep. **141**, 319 (1986).
[10] J. Plata and J. M. Gomez Llorente, J. Phys. A **25**, L303 (1992).
[11] M. Latka, P. Grigolini, and B. J. West, Phys. Rev. A **47**, 4649 (1993).
[12] S. Fishman, D. R. Grempel, and R. E. Prange, Phys. Rev. Lett. **49**, 509 (1982).
[13] R. C. Brown and R. E. Wyatt, Phys. Rev. Lett. **57**, 1 (1986).
[14] G. Casati, B. V. Chirikov, I. Guaneri, and D. L. Shepelyansky, Phys. Rev. Lett. **56**, 2437 (1986).
[15] F. M. Izrailev, Phys. Rep. **196**, 299 (1990).
[16] R. V. Jensen, S. M. Susskind, and M. M. Sanders, Phys. Rep. **201**, 1 (1991).
[17] M. V. Berry, Philos. Trans. R. Soc. London Ser. A **287**, 237 (1977).
[18] J. S. Hutchinson and R. E. Wyatt, Chem. Phys. Lett. **72**, 378 (1980).
[19] H. J. Korsch and M. V. Berry, Physica D **3**, 627 (1981).
[20] Y. Weissman and J. Jortner, J. Chem. Phys. **77**, 1486 (1982).
[21] K. Takahashi and N. Saito, Phys. Rev. Lett. **55**, 645 (1985).
[22] S. J. Chang and K. J. Shi, Phys. Rev. A **34**, 7 (1986).
[23] M. J. Stevens and B. Sundaram, Phys. Rev. A **39**, 2862 (1989).
[24] R. T. Skodje, H. W. Rohrs, and J. Van Burskirk, Phys. Rev. A **40**, 2894 (1989).
[25] R. V. Jensen, M. M. Sanders, M. Saraceno, and B. Sundaram, Phys. Rev. Lett. **63**, 2771 (1989).
[26] W. A. Lin and L. E. Ballentine, Phys. Rev. A **45**, 3137 (1992).
[27] N. Ben-Tal, N. Moiseyev, and H. J. Korsch, Phys. Rev. A **46**, 1669 (1992).
[28] K. Husimi, Proc. Phys. Math. Soc. Jpn. **22**, 264 (1940).
[29] H. W. Lee, Phys. Rev. A (to be published).
[30] E. Wigner, Phys. Rev. **40**, 749 (1932).
[31] W. A. Lin and L. E. Reichl, Physica D **19**, 145 (1986).
[32] L. E. Reichl and W. A. Lin, Phys. Rev. A **33**, 3598 (1986).
[33] J. Y. Shin and H. W. Lee, J. Korean Phys. Soc. **27**, 5 (1994).
[34] Localized and extended states in this work refer to quasienergy states that are located in a given resonance zone. Thus by extended states we mean quasienergy states that lie in the separatrix region of resonance and show significantly more delocalized distributions than the ground state of the Mathieu equation. These are not to be confused with the extended states of some earlier work (e.g., Refs. [11] and [27]) which represent quasienergy states that are located in a classically chaotic region and exhibit delocalized distributions.
[35] D. F. Escande and F. Doveil, J. Stat. Phys. **26**, 257 (1981).

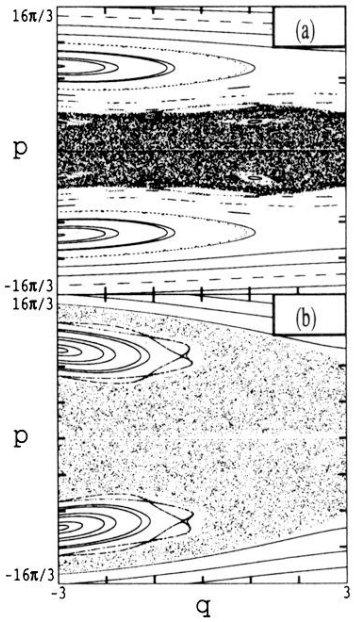

FIG. 1. Classical phase-space map of a particle of mass m in a symmetric infinite square well potential of width $2a$ driven by a sinusoidal force $F = F_0 \cos \omega t$. The parameters are chosen to be $m = 1,\ 2a = 6, \omega = 5$. The amplitude of the driving force is $F_0 = 2$ for (a) and $F_0 = 6$ for (b).